Author Manuscript

Author Manuscript

Author Manuscript

Author Manuscript

HHS Public Access

Author manuscript

J Am Chem Soc. Author manuscript; available in PMC 2020 April 03.

Published in final edited form as:

J Am Chem Soc. 2019 July 10; 141(27): 10821–10829. doi:10.1021/jacs.9b04655.

Networked Communication between Polymerase and Exonuclease Active Sites in Human Mitochondrial DNA Polymerase

Mark L. Sowers[*,†,‡], **Andrew P. P. Anderson**[‡,‖], **James O. Wrabl**[⊥], **Y. Whitney Yin**[*,‡,‖,§]

[†]MD-PhD Combined Degree Program, University of Texas Medical Branch, Galveston, Texas 77555, United States

[‡]Department of Pharmacology and Toxicology, University of Texas Medical Branch, Galveston, Texas 77555, United States

[§]Sealy Center for Structural Biology, University of Texas Medical Branch, Galveston, Texas 77555, United States

[‖]Program of Quantitative and Computational Biosciences, Baylor College of Medicine, Houston, Texas 71115, United States

[⊥]Department of Biology, Johns Hopkins University, 3400 North Charles Street, Baltimore, Maryland 21218, United States

Abstract

High fidelity human mitochondrial DNA polymerase (Pol γ) contains two active sites, a DNA polymerization site (*pol*) and a $3'-5'$ exonuclease site (*exo*) for proofreading. Although separated by 35 Å, coordination between the *pol* and *exo* sites is crucial to high fidelity replication. The biophysical mechanisms for this coordination are not completely understood. To understand the communication between the two active sites, we used a statistical-mechanical model of the protein ensemble to calculate the energetic landscape and local stability. We compared a series of structures of Pol γ, complexed with primer/template DNA, and either a nucleotide substrate or a series of nucleotide analogues, which are differentially incorporated and excised by *pol* and *exo* activity. Despite the nucleotide or its analogues being bound in the *pol*, Pol γ residue stability varied across the protein, particularly in the *exo* domain. This suggests that substrate presence in the *pol* can be "sensed" in the *exo* domain. Consistent with this hypothesis, in silico mutations made in one active site mutually perturbed the energetics of the other. To identify specific regions of the polymerase that contributed to this communication, we constructed an allosteric network connectivity map that further demonstrates specific *pol–exo* cooperativity. Thus, a cooperative network underlies energetic connectivity. We propose that Pol γ and other dual-function

[*]**Corresponding Authors:** mlsowers@utmb.edu; ywyin@utmb.edu.

The authors declare no competing financial interest.

ASSOCIATED CONTENT

Supporting Information

The Supporting Information is available free of charge on the ACS Publications website at DOI: 10.1021/jacs.9b04655.

COREX Monte Carlo calculation reproducibility; differences in SASA between structures; differences in residue stability; diffusely cooperative residues; Pol γ structures used; differences in RMSD; and Pol I BF structures used (PDF)

Author Manuscript Author Manuscript Author Manuscript Author Manuscript

polymerases exploit an energetic coupling network that facilitates domain–domain communication to enhance discrimination between correct and incorrect nucleotides.

Graphical Abstract

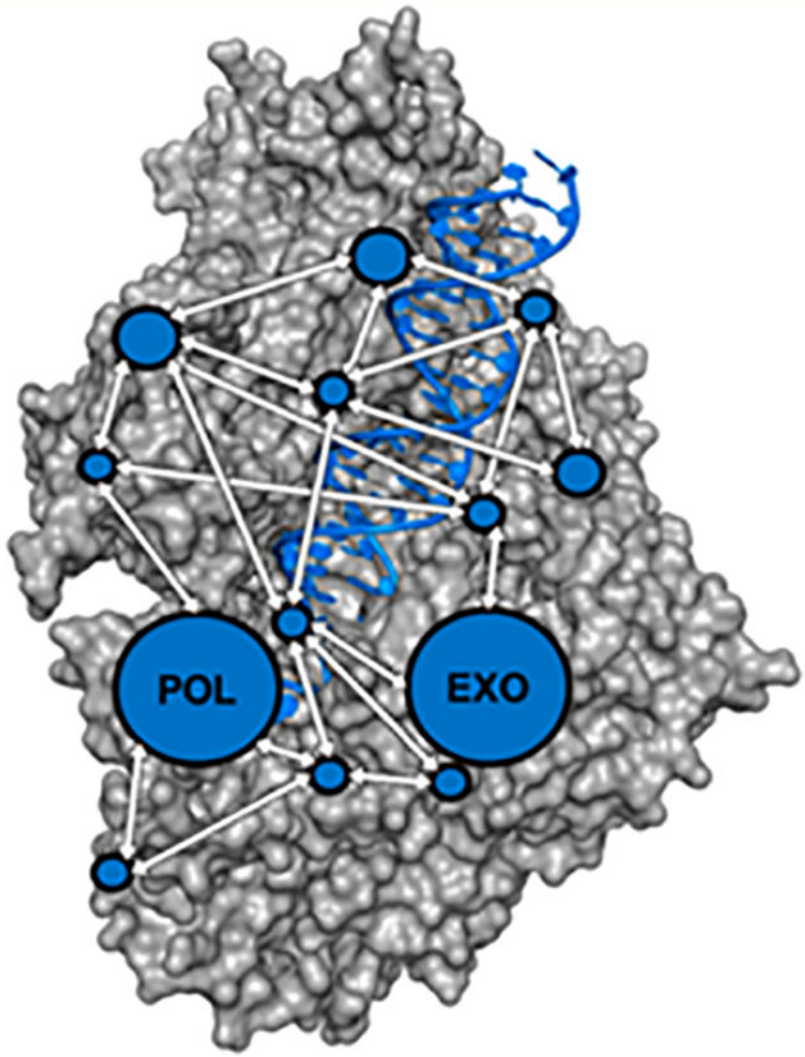

INTRODUCTION

Human mitochondrial DNA polymerase (Pol γ) is responsible for replicating mitochondrial DNA and is vital for organelle function. Pol γ is a heterotrimeric holoenzyme that consists of a catalytic subunit, Pol γA, and a dimeric accessory subunit, Pol γB. Pol γ is a high fidelity polymerase, and all enzymatic activity is fulfilled by Pol γA including polymerization (*pol*), proofreading ($3'-5'$ exonuclease, *exo*), and $5'$-deoxyribose phosphate lyase activities for base excision repair. Although having no enzymatic activity itself, Pol γB regulates all Pol γA activities.[1–3]

Author Manuscript Author Manuscript Author Manuscript Author Manuscript

The *pol* domain adopts a canonical right-hand configuration similar to other Pol I Family members, with subdomains called palm, fingers, and thumb. The palm houses the *pol* catalytic active site, and the fingers are responsible for binding to DNA and incoming deoxynucleotide triphosphates (dNTPs). The thumb likely plays an important role in directing the primer/template to either *pol* or *exo* active sites that are located on two ends of the molecule.[4] Coordination of *pol* and *exo* activity contributes substantially to replication fidelity of Pol γ.

Mutations in the POLG gene are one of the most common causes of inherited mitochondrial disease in several major phenotypes of neurodegenerative disease that include childhood myocerebrohepatopathy spectrum disorders, Alpers syndrome, ataxia neuropathy spectrum disorders, myoclonus epilepsy myopathy sensory ataxia, and progressive external ophthalmoplegia.[5,6] To date, more than 170 Pol γ mutations have been associated with disease symptoms.[7] This is believed to be due to impaired Pol γ function leading to deficits in mitochondrial replication and repair. Ultimately, deficits disrupt mitochondrial function, which is essential in neurons for energy production.[8] Crystal structures of Pol γ and its ternary complex structures provide considerable information to rationalize many mutations; nonetheless, certain mutations are inexplicable. While structures may explain the local effects of mutations, they cannot explain how mutations in *pol* or *exo* active sites, separated by 35 Å, can mutually affect each other's activity. For example, mutations in the finger subdomain can reduce Pol γ DNA synthesis efficiency and elevate exonuclease activity, and mutations in the *exo* simultaneously reduce exonuclease and polymerase activities.[9,10] In addition, one of the most common mutations A467T, distal (~40 Å) to either active site, inhibits *pol* as well as *exo* activity.[11] The phenotypes of these mutants indicate that the two active sites are functionally connected and may be allosterically regulated. However, the structural and molecular basis for such long-range connectivity is unknown.

Pol γ is a major off-target for nucleoside analogue reverse transcriptase inhibitors (NRTIs) designed to inhibit pathogenic human virus HIV, which contributes to their toxicity.[12] NRTIs are prodrugs that must be enzymatically converted to a triphosphate form intracellularly and incorporated by a polymerase into the 3′-end of a growing DNA primer. The *pol* and *exo* active sites of Pol γ recognize NRTIs differently.[13] The catalytic efficiency (k_{pol}/K_d) of cytosine-based NRTIs Zalcitabine (ddC), Lamivudine (3TC), and Emtricitabine (FTC) (Figure 1) varies over 5 orders of magnitude relative to the natural substrate deoxycytidine triphosphate (dCTP), dCTP $\gg$ (+)-FTCTP > ddCTP > (+)-3TCTP > (–)-3TCTP $\gg$ (–)-FTCTP, but the excision rates from primer-DNA by the *exo* site are in a different order, dC > (+)-3TC $\gg$ (–)-FTC $\gg$ ddC.[14,15]

The precise mechanism by which incorrect substrates are differentially recognized is not completely known. The *pol* and *exo* sites are separated by 35 Å, suggesting that communication must be mediated either by a "path" connecting the two active sites or by a large conformational change. Revealing such a connecting path is not only important for understanding the fidelity of the DNA polymerase but also important for developing low toxicity antiviral polymerase inhibitors. The development of analogues that are recognized by HIV reverse transcriptases but rejected by Pol γ, either by *pol* or by *exo*, would be a breakthrough that increases the efficacy and/or decreases the toxicity of NRTI therapy.

Author Manuscript Author Manuscript Author Manuscript Author Manuscript

We have determined several crystal structures of Pol γ, but they have not yet provided a mechanism for how the two active sites communicate and how that may impact polymerase fidelity. We report here computational studies that detect energetic connectivity using a semiempirical statistical mechanical method encoded in the COREX algorithm. We compared a group of Pol γ ternary complex crystal structures with primer/template DNA, and either a substrate dNTP or a NRTI (Figure 1).[4,16] Our study identifies potential two-way communication between the *pol* and *exo* domains. As seen in other allosteric proteins, site–site coupling does not necessarily involve a direct pathway, a series of discrete deformations in contiguous amino acids, but rather occurs through a more diffuse cooperative network that involves all of the subdomains known to be relevant to catalytic activity. Our computational approach detected long-range intramolecular connectivity that cannot be directly revealed by crystal structures alone.

METHODS

COREX Calculations

C source code of COREX was obtained from Professor Vincent Hilser (Johns Hopkins University). COREX calculations were performed on crystal structures of Pol γ holoenzyme ternary complexes with either a nucleotide or an HIV reverse transcriptase inhibitor and a 24/28 nt primer/template DNA 5′-$_{\mathrm{d}}$ $_{\mathrm{d}}$ CATACCGTGACCGGGAGCAAAAGC-3′ and 5′-GCTTTTGCTCCCGGTCACGGTATGGAGC-3′ (Table S1). Structures were prepared by removing nonprotein atoms as well as the accessory subunit, Pol γB. To prevent overestimating contributions of residues with high flexibility (*B*-factor > 100), we eliminated the side chains of these residues and only use their backbone atoms for calculations. These residues are E481, D482, F610, Y649, V742, S759, and C760. In silico mutants were constructed in COOT.[17] The rotamer configuration for each substitution was selected such that there was no steric clash. Thermostable *Bacillus* DNA Polymerase I large fragment (Pol I BF) structures were prepared similarly.

Briefly, COREX generates a conformational ensemble from a given three-dimensional structure. This is accomplished by systematically unfolding small “windows” of residues in the fully folded structure. The unfolding of that set of residues exhibits a change in solvent accessible surface area (SASA), composed of the area gained from unfolding the residues plus any newly exposed interfacial surface.[18] This interfacial surface is key to the algorithm’s ability to model distant cooperative unfolding events that might be involved in long-distance communication. The free energy (ΔG_i) of each conformational permutation *i*, or microstate, is then calculated on the basis of previously determined empirical equations that link changes in SASA to thermodynamic parameters.[18] Probabilities (P_i) of any given microstate are then determined using the partition function *Q*, which is the sum of all microstate energies (eq 1):

$$P_i = \frac{e^{-\Delta G_i / RT}}{Q} \quad (1)$$

where *R* is the universal gas constant and *T* is temperature in kelvin. The primary output used is a residue stability or folding constant, $K_{\mathrm{f},j}$, defined as the ratio of the summed

Author Manuscript Author Manuscript Author Manuscript Author Manuscript

probability in which a particular residue *j* is folded ($\sum Pf_j$) over all microstates divided by the summed probability of all states in which that residue is unfolded ($\sum Puf_j$) as shown in eq 2:

$$K_{f,j} = \frac{\Sigma Pf_j}{\Sigma Puf_j} \quad (2)$$

This value is an estimated equilibrium constant for unfolding at every residue position, which can be converted to a free energy of stability by the relation $\Delta G = -RT \ln K_{f,j}$. As such, these calculations have been verified by direct comparison to hydrogen exchange protection factors.[19]

The Monte Carlo sampling version of COREX was used, and the source was further modified to allow for the large size of Pol γA by modifying the following variables: Max_Res to 6000, Max_Atoms to 50000, and Max_Nunits to 1000. Specific parameters used for the calculation include a window size of 50 residues, a minimum window size of 40 residues, and 5000 samples per partition. The partition refers to the "sliding window" approach used in COREX to generate microstates. The first partition is the first 50 residues from the N-terminus of Pol γA, and each following 50 residues is another window, for a total of 24 windows that can be either "folded" or "unfolded". The windows then were incremented by one residue, and another 24 windows were generated. The sliding was iterated until the first window on the N-terminus was moved to the 50th residue, generating a total of 50 partitions. We sampled 5000 microstates in each partition for a total of 250 000 microstates in the simulated ensemble. To test the sufficiency of sampling, crystal structures were also run with the same parameters but a larger sampling size of 50 000. Residues 505–539 were under-sampled, and no values were calculated, due to their highly solvent accessible surface area. *Pol* I binary complexes were run similarly with 1000 samples per partition.

Residue Stability Variance

Differences between the different ternary complexes or in silico mutations were obtained by computing the standard deviation of residue stability ($K_{f,j}$) between the same residue across all structures, for all residues in Pol γA.

Allosteric Connectivity Map

To construct the allosteric network connectivity map using the single site thermodynamic mutation algorithm,[22] the ensemble data generated as described above were used. A 1 kcal/mol stabilizing energy, **Φ**, then was applied to each microstate in which a given residue, *k*, was found folded. Then we estimated how perturbing residue *k* affected the residue stability of the *j*th residue in the protein, $K_{f,j}$, as encompassed in eq 3.

$$K_{f,j}^{Mutk} = \frac{\Phi \cdot \sum Pf_{jlk} + \sum Pf_{jluf,k}}{\Phi \cdot \sum Puf_{jlf,k} + \sum Puf_{jluf,k}} \quad (3)$$

Author Manuscript Author Manuscript Author Manuscript Author Manuscript

RESULTS

Crystal Structures

3-D structures of catalytic subunit Pol γA were taken from holoenzyme ternary complexes containing an identical 24/28 nucleotide primer/template DNA with a 3′-dideoxy-terminated primer to prevent elongation, and a dNTP or an analogue: dCTP, or a triphosphate form of cytosine-based NRTI, Zalcitabine (ddC), Emtricitabine (–)-FTC, or the chiral enantiomer (+)-FTC (Table S1). Pol γA in the crystal structures is an exonuclease-deficient double mutant (D198A/E200A).

COREX Analysis of Pol γ Complexes Containing dCTP or NRTIs

To investigate energetic fluctuations as a possible cause for the different kinetics and binding affinities, residue stability constants (ln $K_{f,j}$, eq 2) were calculated for the four Pol γ ternary complex structures. Each complex was sampled with 250 000 microstates. To ensure sufficient sampling, we computed ln $K_{f,j}$ for the structure at a larger sampling size of 2 500 000 microstates. The results from the two calculations are consistent (Figure S1), suggesting that sampling of 250 000 microstates sufficiently captured features of the entire ensemble.

Population standard deviation (S.D.) of residue stability was determined to reveal the difference in stability between the four different ligand-bound Pol γ ternary complexes (Figure 2). Neglecting the termini, because they tend to be highly flexible and under-sampled, six regions named ranges A–F were shown to contain variability greater than the mean (Figure 2A,B).

While any changes in residue stability are meaningful, we focus on the regions that exhibit high variability. We mapped these regions onto the ternary complex containing dCTP (PDB: 4ZTZ).[21] The biological significance of the perturbed regions is immediately obvious (Figure 2A–D). Ranges A and B are found within the *exo* domain in conserved motifs.[20] Range B contains *exo* motif III and a portion of the thumb subdomain, and range C includes the remainder of the thumb. Ranges D–F comprise parts of both the *pol* catalytic palm and the fingers subdomain that binds to DNA and incoming nucleotide (Figure 2C,D). Interestingly, both local and distal energetic residue stability fluctuates with different ligands (dNTP/NRTIs). For example, on the backside of the catalytic subunit, behind where DNA binds, a portion of the thumb domain is found to be perturbed. This region also interacts with one of the accessory subunits, Pol γB (Figure 2C). Nonetheless, most of the perturbed residues lie between the *pol* and *exo* active sites where the elongating primer/template DNA resides (Figure 2D, DNA not shown). While perturbation of residues in the local *pol* active site would be expected, the largest variations were seen in the remote *exo* domain, in range B. This implies a compensatory coupling between *exo* and *pol* sites. The results suggest the existence of a cooperative network that transmits information from the active site to one or more regions of the protein.

The stability constant $K_{f,j}$ provides an orthogonal measurement to the structural information in a crystal. The complexes with dCTP and ddCTP are highly similar to a RMSD of 0.019 Å (Table S2). However, due to subtle differences in side chain conformation that affect SASA (Figure S2), the residue stability differences can be revealed by $K_{f,j}$ values (Figure S3).

Author Manuscript Author Manuscript Author Manuscript Author Manuscript

Impact of in Silico Mutations on the Energetic Coupling between *pol* and *exo* Sites

To further explore *pol*–*exo* communication, we took advantage of naturally occurring POLG mutations associated with human diseases to probe this potential connectivity. We chose deleterious *exo* motif III and thumb mutations, G426S, L424G/G431 V, L428P/A467T, and A467T, as well as *pol* finger subdomain mutations, Y955C, A957S, and Y955C/A957S. In Pol γ, binding of incoming nucleotide dNTP is accomplished by two helices: the O-helix that interacts with the dNTP and the O1-helix that stabilizes the helix-turn-helix motif.

Y955 is located on the nucleotide binding O-helix and is proposed to be involved in dNTP selection. A957 is located on the connecting loop between the O- and O1-helix. Both helices undergo open-to-closed conformational changes when the correct dNTP is bound.[4]

Mutations A957S and A957P were analyzed by pre-steady-state kinetics on a single nucleotide incorporation assay and electrophoretic mobility shift assay.[23] The results show that the substitutions of A957 with Serine or Proline reduced catalytic efficiency by 1.8- and 60-fold, respectively, largely due to reduced dNTP binding in the *pol* site. Mutant Y955C displayed a similar phenotype, with a 46-fold reduced K_M to the incoming nucleotide without significantly altering catalytic rates.[24] Thus, both Y955 and A957 contribute substantially to substrate dNTP binding affinity. As they do not directly interact with dNTP, their effects are likely mediated by alteration of the conformational ensemble.

Residue stability and its SD were calculated for both sets of *exo* (G426S, L424G/G431 V, L428P/A467T, and A467T) and *pol* mutations (Y955C, A957S, and Y955C/A957S) relative to the wild-type (wt) complex such that the variance in residue stability is a relative measurement of deviation from the wt complex. *Exo* mutants and *pol* mutants, relative to wt, are shown in green and red, respectively (Figure 3A). *Exo* mutants show local fluctuations in range B. However, large energetic variation is unexpectedly seen in the distal fingers, adjacent to the *pol* active site (Figure 3A–C). We also observed that a perturbation in the *pol* domain affects the *exo*, as shown by the red peaks in ranges A and B (Figure 3A). The finger residues ~900–1050, referred to as the new hypervariable region (NHR), were the most perturbed residues of the *pol* domain. This span of residues includes portions of ranges D and E that were identified as hypervariable across structures with different substrates bound. When previously comparing different crystal structures, the residues between ranges D and E comprised one of the least variable portions of the protein. However, here we show that both catalytic site *pol* or *exo* mutations affect this region. This suggests that this region is important intrinsically for *pol*–*exo* communication, although it is not differentially affected by cytosine-based NRTI binding. Also, *exo* mutant perturbations had a pattern similar to that of *pol* mutants, implying a similar pattern of cooperativity (Figure 3A).

These results provide additional supporting evidence that the two active sites are energetically coupled.

Allosteric Network Connectivity Map Using Single Site Thermodynamic Mutations

Thus far, we have demonstrated there is energetic coupling between Pol γ *pol* and *exo* by observing the mutual change of stability in one active site when the other is perturbed by mutations or different ligands. To investigate whether such mutual effects are specific to the

Author Manuscript Author Manuscript Author Manuscript Author Manuscript

active sites, we thermodynamically perturbed each residue in our COREX ensemble using a single site thermodynamic mutation algorithm (eq 3).[22] If a region remote to a perturbed region alters its energetics in response to the perturbation, it is said to have cooperativity with the perturbed region. If the energetic changes of the remote and perturbed regions are in sync, the two sites are positively coupled; if the energetic changes are in anti-sync, the two sites are negatively coupled. In all other situations, the two sites are not related. The diagonal area of the map represents self-cooperativity of local regions of 10–20 residues.

The operation yielded an allosteric network connectivity map that reveals that not all regions or residues are cooperative with other residues, and that only limited regions show connectivity. Nearly all residues in the *pol* finger subdomain are positively coupled to regions within the *exo* and the N-terminal domain (Figure 4). This includes residues corresponding to,or near those, in which we found to be hypervariable either by in silico mutations or with different ligands such as range B/motif III, the *exo* active site (D198/200), and residues 300–375. Additionally, fingers subdomain mutations selected, Y955 and A957, are located in the region that is highly coupled with the *exo* domain (Figure 4). This region also contains mutation R964C, which was discovered in AIDS patients with elevated NRTI toxicity.[25] This mutation displays only slightly reduced *pol* activity but nearly abolished *exo* activity,[9] confirming the specificity of energetic coupling between the *pol* and *exo* sites. The biochemical results suggest drug toxicity may be caused by defective *exo* activity as the erroneously incorporated NRTI cannot be excised, due to disrupted *pol*–*exo* communication.

Other regions showing coupling are mutational clusters that have been identified in patients. Previously defined clusters are *pol* active site and its environs (1), upstream DNA-binding channel (2), altered *exo*:*pol* ratio (3), distal accessory subunit interface (4), and protein–protein interactions (5).[7] Mutation cluster 3 is hypothesized to regulate *pol* and *exo* activities, and contains the “partitioning loop” believed to partition DNA in either active site.[4] Portions of cluster 3 are found within the fingers subdomain, a region that is highly coupled with large regions of the *exo* and N-terminal domains (Figure 4). This analysis supports our results that either differential ligand binding or mutations can perturb both *pol* and *exo* domains. It also suggests active site communication is specific, as perturbations of many other regions do not change the energetics of either active site (Figure 4). Conversely, most cluster 1 mutations found in the *pol* domain, which are believed to only affect the *pol*, appear not to affect other domains, as expected. Similarly, cluster 4 substitution mutations do not affect other residues in the A subunit. As this cluster does not appear to be cooperative with other regions in Pol γA, perhaps it most likely affects the accessory subunit Pol γB, as predicted.

The spacer domain appears to be highly self-cooperative, as demonstrated by the large stretch of ~150 amino acids highly positively coupled (the red block in the center of Figure 4). This is particularly interesting as this region is believed to stabilize the interaction with DNA as well as the accessory subunits. Self-cooperativity of this large stretch may facilitate rapid and large conformational changes upon DNA binding.

Some mutational clusters fall into regions that appear highly coupled to the entire protein, including most of clusters 2 and 5. Cluster 2 mutations affect DNA binding, suggesting that

Author Manuscript Author Manuscript Author Manuscript Author Manuscript

mutations in the cluster might disrupt coordination of DNA binding with conformational changes necessary for correct nucleotide selection. Although separated by primary sequence, these regions are structurally adjacent and interact both with DNA and with the processivity subunit (Figure S4). This raises the possibility that allostery in the overall system may in part be mediated by DNA itself, a conclusion supported by the large conformational changes seen when comparing the holoenzyme structure, which contains no ligand or DNA (PDB ID: 3IKM), to the ternary complex (PDB ID: 4ZTZ).

Energetic Coupling in Another Pol I Family Polymerase, *Pol* I BF

To investigate whether or not our findings in Pol γ are innate to the structural features of this family of polymerases, we performed the same analyses on another Pol I Family member, thermostable *Bacillus* DNA Polymerase I large fragment (Pol I BF). Pol I BF shares the same right-hand conformation with fingers (residues 656–815), thumb (residues 496–595), and palm (residues 617–655 and 830–869) subdomains that constitute the *pol* domain. It also contains a vestigial $3'-5'$ exonuclease domain (302–468).[26,27]

To better understand *pol*–*exo* communication under physiological situations, we compared Pol I BF bound to either a correctly matched or a mismatched primer/template DNA. A mismatch in *pol*, resulting from incorporation of an incorrect nucleotide, should engage the *exo* site for mismatch removal. Comparison of the energetics of Pol I BF with a matched or mismatched primer/template DNA, using the binary complex crystal structures (Table S3),[28] reveals that differences are concentrated in four regions: I (residues 350–388), II (residues 478–515), III (residues 581–658), and IV (689–780 and 802–817) (Figure 5A,B). Region I contains the conserved *exo* motif III, and region IV is in the fingers subdomain. The fingers subdomain undergoes conformational changes with each nucleotide addition. It adapts mostly an open conformation in the absence of dNTP, and changes to ajar and or closed conformations in the presence of an incorrect or a correct nucleotide, respectively.[27,29,30] Our results in Figure 4 suggest that in most conformations, captured by our ensemble calculations, the fingers domain is strongly coupled with the *exo* motif III region. The results from Pol I BF are in good agreement with those from Pol γ, suggesting that this mode of communication is conserved within Pol I family members.

DISCUSSION

Allosteric Regulation of *pol* and *exo* Sites

Pol γ *pol* and *exo* sites have distinct enzymatic activities that are highly coordinated during DNA replication. This coordination is critical for correct dNTP discrimination. The *pol* site selects for the correct nucleotide and catalyzes phosphodiester bond formation to extend the primer DNA, while the *exo* hydrolyzes the primer $3'$-end. If a correct nucleotide is incorporated, the enzyme retains the primer DNA in the *pol* for continued synthesis. If an incorrect nucleotide is incorporated, mismatched primer/template DNA is transferred to the *exo* for removal. Crosstalk between these sites in DNA polymerases is known to be an important contributor to the fidelity of DNA replication. The biophysical basis for signal transduction from misincorporation in the *pol* to the distal *exo* site is not fully understood. *Pol* and *exo* site coordination is also critical for discrimination of NRTIs from normal

Author Manuscript Author Manuscript Author Manuscript Author Manuscript

dNTPs. Otherwise, misincorporation of an NRTI into mitochondrial DNA can result in drug toxicity. Understanding active site coordination and its role in discriminating between these inhibitors is critical to both improving drug efficacy and decreasing toxicity.

In this study, we report positive cooperativity between the fingers subdomain of the *pol* and conserved motif III of the *exo* domain. Perturbation of the *pol*, by either mismatched primer, NRTI inhibitor, or a mutation, can stimulate a corresponding perturbation in the *exo*, indicating energetic coupling between the two regions. Similar findings in Pol I BF suggest that this communication may be intrinsic to their conserved structure and sequence, in two evolutionarily divergent but structurally homologous polymerases. The positive cooperativity between the *pol* finger subdomain and *exo* is particularly intriguing as the fingers directly interacts with the incoming dNTP and contributes to correct nucleotide selection through open-closed conformational changes.[31]

A multitude of factors contribute to correct nucleotide dNTP selection including hydrogen bonding with the templating nucleobase, steric interactions, nucleotide sugar conformation, and polymerase conformational changes.[27,31,32] Nucleotides can also influence polymerase conformation in a series of distinct steps both before and during covalent bond formation.[33] Even nucleotide interactions with DNA template and solvent can have profound impacts on nucleotide selection.[34,35] Quantum mechanical/molecular modeling studies of human Pol β revealed that residues surrounding the *pol* active site, referred to as base-binding residues, contribute to the transition state of dNTP incorporation.[36–38] Furthermore, the study found incorrect dNTP can perturb the *pol* active site and form a nonproductive transition state, indicating that both dNTP and *pol* residues contribute to stability and reactivity. Our conclusions are not only in agreement with those concerning Pol β, but they also suggest that ligand binding and perturbations in the *pol* can be propagated to the distal *exo* site. Pol β is a DNA repair polymerase without *exo* activity. Whether changes to its *pol* site are propagated to other regions is unknown.

For dual active site polymerases, DNA transfer during replication between *pol* and *exo* active sites is necessary to achieve high fidelity. Our work here suggests that inter- and intradomain cooperativity may facilitate two innate fidelity checkpoints: *pol–exo* sampling and finger subdomain conformational changes (open/closed/ajar), respectively.[31,39] Studies of *Escherichia coli* DNA Pol I Klenow fragment (KF) showed that both DNA intramolecular and intermolecular transfer between active sites coexist, but intramolecular transfer is the faster of the two pathways.[39] Importantly, mismatched DNA preferentially associates with the *exo* site, and even more so in the presence of dNTP. In agreement with our study, this suggests that *pol–exo* cooperativity may facilitate transitioning the polymerase to its proofreading mode when bound to mismatched DNA, and to its synthesis mode when bound to correctly matched DNA, and dNTP ligand can further influence this coordination.

Pol and *exo* active sites are spatially separated by 35 Å. This begs the question: How does their long-range coupling occur? Our COREX calculations are based on an ensemble model that proposes allostery is the result of changes in the conformational distribution, rather than a distinct linear pathway of contiguous amino acids or really any clearly defined “path”.[40] Allosteric regulation of remote sites can be attributed to ligand-induced entropic changes

Author Manuscript Author Manuscript Author Manuscript Author Manuscript

and thermodynamic fluctuation, and/or to transitions in structural ensembles. Other studies also suggest that “paths” for allostery are diffuse, nonlinear, and nonlocal; they have also been described as an elastic network where soft collective modes of motion enable allosteric regulation of protein systems.[41–44]

Equilibrium of Conformational Populations

COREX allows estimation of a protein’s local stability at single residue resolution.[18] An advantage is the generation of a thermodynamic ensemble of conformational microstates that reasonably models the additional degrees of freedom not obvious in crystal structures. For example, DNA polymerases undergo conformational fluctuations, mutations, DNA, and or dNTP binding influences the proportions of predominant conformations.[30,45] We simulate these many possible conformations, constructed an appropriate partition function, and weighted them by their respective probabilities. COREX has also been used in describing cryptic long-range energetic connectivity in other systems, revealing the energetic consequences of subtle structural differences.[46–48] Our analyses of Pol γ suggest that ensemble-based energetic coupling facilitates coordination between different functional domains.

New Evaluation Tool for Pol γ Mutations

Pol γ mutations have been implicated in many human diseases. Deficient polymerase activity reduces mitochondrial DNA replication, decreases mitochondrial DNA copy number, and hampers cellular energy supply. Our studies suggest that COREX is particularly useful in analyzing mutational effects. Starting with the ground state of the enzyme in its native structure, the algorithm, although unable to provide dynamics, readily reveals that perturbations of one region can affect the stability of other regions.

Pol γ mutations associated with disease are located in and around the active sites of *pol* and *exo*, as well as at noncatalytic sites. While crystal structures are invaluable in analyzing local effects of amino acid substitutions, they do not explain long-range effects of mutations and either intra- or interdomain communication. Our approach here suggests mutations or ligands that affect residue stability in distal regions do so through population changes in the conformational ensemble. As a result, COREX affords a new approach for mutational analyses. Perturbations can be revealed computationally to propagate over long distances across the molecule via newly exposed interfaces without the initiating and terminal sites being in direct contact. For example, the connectivity map analyses presented here show that the stability of some localized clusters of disease-associated mutants, distal to either active site, is associated with the stability of the entire enzyme as well as *pol*–*exo* communication. COREX can therefore provide an energetic explanation for the dysfunction of these Pol γ mutants. As a major adverse target for NRTIs, Pol γ mutations can alter the drug toxicity in different patients.[49,50] Our results here should be an effective tool to screen potential NRTI response in the more than 400 single nucleotide polymorphisms (SNPs) in POLG (http://exac.broadinstitute.org/gene/ENSG00000140521). The network of local and nonlocal perturbations induced by POLG variants and NRTIs, as revealed by COREX, may facilitate personalized treatments for patients based on their POLG genotype.

Author Manuscript Author Manuscript Author Manuscript Author Manuscript

CONCLUSION

This study provides the first examination of energetic coupling, where perturbations in the *pol* site are sensed by the *exo*, in the high-fidelity mitochondrial DNA polymerase, Pol γ. We demonstrated that substrate nucleotide or nucleotide analogue (NRTIs), as well as Pol γ amino acid substitutions, perturb a complex network, resulting in local and nonlocal perturbations. Our results have provided a biophysical basis for communication between *pol* and *exo* sites of Pol γ, suggesting that COREX is a powerful tool to analyze mutational effects of both local and remote regions of a protein.

Supplementary Material

Refer to Web version on PubMed Central for supplementary material.

ACKNOWLEDGMENTS

We thank V. J. Hilser, J. C. Lee, and L. C. Sowers for helpful comments. The work was supported in part by grants from the NIH (GM110591 and AI134611) to Y.W.Y. and from the Sealy and Smith Foundation to Sealy Center for Structural Biology at UTMB.

REFERENCES

(1). Gray H; Wong TW Purification and Identification of Subunit Structure of the Human Mitochondrial DNA Polymerase. J. Biol. Chem 1992, 267, 5835–5841. [PubMed: 1556099]

(2). Johnson AA; Johnson KA Exonuclease Proofreading by Human Mitochondrial DNA Polymerase. J. Biol. Chem 2001, 276, 38097–38107. [PubMed: 11477094]

(3). Johnson AA; Johnson KA Fidelity of Nucleotide Incorporation by Human Mitochondrial DNA Polymerase. J. Biol. Chem 2001, 276, 38090–38096. [PubMed: 11477093]

(4). Szymanski MR; Kuznetsov VB; Shumate C; Meng Q; Lee Y-SY-S; Patel G; Patel S; Yin YW Structural Basis for Processivity and Antiviral Drug Toxicity in Human Mitochondrial DNA Replicase. EMBO J. 2015, 34 (14), 1959–1970. [PubMed: 26056153]

(5). Rahman S; Copeland WC POLG-Related Disorders and Their Neurological Manifestations. Nat. Rev. Neurol 2019, 15 (1), 40–52. [PubMed: 30451971]

(6). Wong LC; Naviaux RK; Brunetti-pierri N; Zhang Q; Schmitt ES; Truong C; Milone M; Cohen BH; Wical B; Ganesh J; Basinger AA; Burton BK; Swoboda K; Gilbert DL; Vanderver A; Saneto RP; Maranda B; Arnold G; Abdenur JE; Waters PJ; Copeland WC Molecular and Clinical Genetics of Mitochondrial Diseases Due to POLG Mutations. Hum. Mutat 2008, 29 (9), E150–E172. [PubMed: 18546365]

(7). Nurminen A; Farnum GA; Kaguni LS Pathogenicity in POLG Syndromes: DNA Polymerase Gamma Pathogenicity Prediction Server and Database. BBA Clin. 2017, 7 (February), 147–156. [PubMed: 28480171]

(8). Zheng X; Boyer L; Jin M; Mertens J; Kim Y; Ma L; Ma L; Hamm M; Gage FH; Hunter T Metabolic Reprogramming during Neuronal Differentiation from Aerobic Glycolysis to Neuronal Oxidative Phosphorylation. Elife 2016, 5, 1–25.

(9). Kasahara T; Ishiwata M; Kakiuchi C; Fuke S; Iwata N; Ozaki N; Kunugi H; Minabe Y; Nakamura K; Iwata Y; Fujii K; Kanba S; Ujike H; Kusumi I; Kataoka M; Matoba N; Takata A; Iwamoto K; Yoshikawa T; Kato T Enrichment of Deleterious Variants of Mitochondrial DNA Polymerase Gene (POLG1) in Bipolar Disorder. Psychiatry Clin. Neurosci 2017, 71 (8), 518–529. [PubMed: 27987238]

(10). Bratic A; Kauppila TES; Macao B; Grönke S; Siibak T; Stewart JB; Baggio F; Dols J; Partridge L; Falkenberg M; Wredenberg A; Larsson NG Complementation between Polymerase- and Exonuclease-Deficient Mitochondrial DNA Polymerase Mutants in Genomically Engineered Flies. Nat. Commun 2015, 6, 1.

Author Manuscript Author Manuscript Author Manuscript Author Manuscript

(11). Chan SSL; Longley MJ; Copeland WC; Carolina N Common A467T Mutation in the Human Mitochondrial DNA Polymerase (POLG) Compromises Catalytic Efficiency and Interaction with the Accessory Subunit * 2005, 280, 31341–31346.

(12). Lewis W; Day BJ; Copeland WC Mitochondrial Toxicity of Nrti Antiviral Drugs: An Integrated Cellular Perspective. Nat. Rev. Drug Discovery 2003, 2 (10), 812–822. [PubMed: 14526384]

(13). Glesby MJ Overview of Mitochondrial Toxicity of Nucleoside Reverse Transcriptase Inhibitors. Int. AIDS Soc 2002, 42–46.

(14). Anderson KS A Transient Kinetic Approach to Investigate Nucleoside Inhibitors of Mitochondrial DNA Polymerase γ. Methods 2010, 51 (4), 392–398. [PubMed: 20573564]

(15). Hanes JW; Johnson KA Exonuclease Removal of Dideoxycytidine (Zalcitabine) by the Human Mitochondrial DNA Polymerase. Antimicrob. Agents Chemother 2008, 52 (1), 253–258. [PubMed: 17984232]

(16). Sohl CD; Szymanski MR; Mislak AC; Shumate CK; Amiralaei S; Schinazi RF; Anderson KS; Yin YW; Sohl CD; Szymanski MR; Mislak AC; Shumate CK; Amiralaei S Probing the Structural and Molecular Basis of Nucleotide Selectivity by Human Mitochondrial DNA Polymerase γ. Proc. Natl. Acad. Sci. U. S. A 2015, 113 (5), E662–E662.

(17). Emsley P; Lohkamp B; Scott WG; Cowtan K Features and Development of Coot. Acta Crystallogr. Sect. D Biol. Crystallogr 2010, 66 (4), 486–501. [PubMed: 20383002]

(18). Hilser VJ; Freire E Structure-Based Calculation of the Equilibrium Folding Pathway of Proteins. Correlation with Hydrogen Exchange Protection Factors. J. Mol. Biol 1996, 262 (5), 756–772. [PubMed: 8876652]

(19). Hilser VJ; García-Moreno E B; Oas TG; Kapp G; Whitten ST A Statistical Thermodynamic Model of the Protein Ensemble. Chem. Rev 2006, 106 (5), 1545–1558. [PubMed: 16683744]

(20). Shevelev IV; Hübscher, U. The 3′−5′ Exonucleases. Nat. Rev. Mol. Cell Biol 2002, 3 (5), 364–375. [PubMed: 11988770]

(21). Lee YS; Kennedy WD; Yin YW Structural Insight into Processive Human Mitochondrial DNA Synthesis and Disease-Related Polymerase Mutations. Cell 2009, 139 (2), 312–324. [PubMed: 19837034]

(22). Hilser VJ; Dowdy D; Oas TG; Freire E The Structural Distribution of Cooperative Interactions in Proteins: Analysis of the Native State Ensemble. Proc. Natl. Acad. Sci. U. S. A 1998, 95 (17), 9903–9908. [PubMed: 9707573]

(23). Sohl CD; Kasiviswanathan R; Copeland WC; Anderson KS Mutations in Human DNA Polymerase γ Confer Unique Mechanisms of Catalytic Deficiency That Mirror the Diease Severity in Mitochondrial Disorder Patients. Hum. Mol. Genet 2013, 22 (6), 1074–1085. [PubMed: 23208208]

(24). Ponamarev MV; Longley MJ; Nguyen D; Kunkel TA; Copeland WC Active Site Mutation in DNA Polymerase γ Associated with Progressive External Ophthalmoplegia Causes Error-Prone DNA Synthesis. J. Biol. Chem 2002, 277 (18), 15225–15228. [PubMed: 11897778]

(25). Yamanaka H; Gatanaga H; Kosalaraksa P; Matsuoka-Aizawa S; Takahashi T; Kimura S; Oka S Novel Mutation of Human DNA Polymerase γ Associated with Mitochondrial Toxicity Induced by Anti-HIV Treatment. J. Infect. Dis 2007, 195 (10), 1419–1425. [PubMed: 17436221]

(26). Kiefer JR; Mao C; Hansen CJ; Basehore SL; Hogrefe HH; Braman JC; Beese LS Crystal Structure of a Thermostable Bacillus DNA Polymerase I Large Fragment at 2.1 A Resolution. Structure 1997, 5 (1), 95–108. [PubMed: 9016716]

(27). Miller BR; Beese LS; Parish CA; Wu EY The Closing Mechanism of DNA Polymerase I at Atomic Resolution. Structure 2015, 23 (9), 1609–1620. [PubMed: 26211612]

(28). Johnson SJ; Beese LS Structures of Mismatch Replication Errors Observed in a DNA Polymerase. Cell 2004, 116 (6), 803–816. [PubMed: 15035983]

(29). Wu EY; Beese LS The Structure of a High Fidelity DNA Polymerase Bound to a Mismatched Nucleotide Reveals an “Ajar” Intermediate Conformation in the Nucleotide Selection Mechanism. J. Biol. Chem 2011, 286 (22), 19758–19767. [PubMed: 21454515]

(30). Hohlbein J; Aigrain L; Craggs TD; Bermek O; Potapova O; Shoolizadeh P; Grindley NDF; Joyce CM; Kapanidis AN Conformational Landscapes of DNA Polymerase I and Mutator Derivatives Establish Fidelity Checkpoints for Nucleotide Insertion. Nat. Commun 2013, 4, 1–11.

Author Manuscript Author Manuscript Author Manuscript Author Manuscript

(31). Berezhna SY; Gill JP; Lamichhane R; Millar DP Single-Molecule Förster Resonance Energy Transfer Reveals an Innate Fidelity Checkpoint in DNA Polymerase I. J. Am. Chem. Soc 2012, 134 (27), 11261–11268. [PubMed: 22650319]

(32). Williams AA; Darwanto A; Theruvathu JA; Burdzy A; Neidigh JW; Sowers LC Impact of Sugar Pucker on Base Pair and Mispair Stability. Biochemistry 2009, 48 (50), 11994–12004. [PubMed: 19899814]

(33). Bermek O; Grindley NDF; Joyce CM Prechemistry Nucleotide Selection Checkpoints in the Reaction Pathway of DNA Polymerase I and Roles of Glu710 and Tyr766. Biochemistry 2013, 52 (36), 6258–6274. [PubMed: 23937394]

(34). Petruska J; Sowers LC; Goodman MF Comparison of Nucleotide Interactions in Water, Proteins, and Vacuum: Model for DNA Polymerase Fidelity. Proc. Natl. Acad. Sci. U. S. A 1986, 83 (6), 1559–1562. [PubMed: 3456600]

(35). Petruska J; Goodman MF; Boosalis MS; Sowers LC; Cheong C; Tinoco I Comparison between DNA Melting Thermodynamics and DNA Polymerase Fidelity. Proc. Natl. Acad. Sci. U. S. A 1988, 85 (17), 6252–6256. [PubMed: 3413095]

(36). Xiang Y; Oelschlaeger P; Floria J; Goodman MF; Warshel A Simulating the Effect of DNA Polymerase Mutations on Transition-State Energetics and Fidelity: Evaluating Amino Acid Group Contribution and Allosteric Coupling for Ionized Residues in Human Pol †. Biochemistry 2006, 45, 7036–7048. [PubMed: 16752894]

(37). Kamerlin SCLL; Warshel A; Kolmodin K The Empirical Valence Bond Model: Theory and Applications. Wiley Interdiscip. Rev. Comput. Mol. Sci 2011, 1 (1), 30–45.

(38). Warshel A; Weiss RM An Empirical Valence Bond Approach for Comparing Reactions in Solutions and in Enzymes. J. Am. Chem. Soc 1980, 102 (20), 6218–6226.

(39). Lamichhane R; Berezhna SY; Gill JP; Van Der Schans E; Millar DP Dynamics of Site Switching in DNA Polymerase. J. Am. Chem. Soc 2013, 135 (12), 4735–4742. [PubMed: 23409810]

(40). Cooper A; Dryden DTF Allostery without Conformational Change - A Plausible Model. Eur. Biophys. J 1984, 11 (2), 103–109. [PubMed: 6544679]

(41). Wodak SJ; Paci E; Dokholyan NV; Berezovsky IN; Horovitz A; Li J; Hilser VJ; Bahar I; Karanicolas J; Stock G; Hamm P; Stote RH; Eberhardt J Allostery in Its Many Disguises: From Theory to Applications. Struct. Rev 2019, 27, 566–578.

(42). Buchenberg S; Sittel F; Stock G Time-Resolved Observation of Protein Allosteric Communication. Proc. Natl. Acad. Sci. U. S. A 2017, 114 (33), E6804–E6811. [PubMed: 28760989]

(43). Motlagh HN; Wrabl JO; Li J; Hilser VJ The Ensemble Nature of Allostery. Nature 2014, 508 (7496), 331–339. [PubMed: 24740064]

(44). Urbanc B Protein Actions: Principles and Modeling by I. Bahar, R.L. Jernigan, and K.A. Dill. J. Biol. Phys 2017, 43 (4), 585–589.

(45). Santoso Y; Joyce CM; Potapova O; Le Reste L; Hohlbein J; Torella JP; Grindley NDF; Kapanidis AN Conformational Transitions in DNA Polymerase I Revealed by Single-Molecule FRET. Proc. Natl. Acad. Sci. U.S.A 2010, 107, 715–720. [PubMed: 20080740]

(46). Maillard RA; Liu T; Beasley DWC; Barrett ADT; Hilser VJ; Lee JC Thermodynamic Mechanism for the Evasion of Antibody Neutralization in Flaviviruses. J. Am. Chem. Soc 2014, 136 (29), 10315–10324. [PubMed: 24950171]

(47). Pan H; Lee JC; Hilser VJ Binding Sites in Escherichia Coli Dihydrofolate Reductase Communicate by Modulating the Conformational Ensemble. Proc. Natl. Acad. Sci. U. S. A 2000, 97 (22), 12020–12025. [PubMed: 11035796]

(48). Li J; White JT; Saavedra H; Wrabl JO; Motlagh HN; Liu K; Sowers J; Schroer TA; Thompson EB; Hilser VJ; Brad Thompson E; Hilser VJ Genetically Tunable Frustration Controls Allostery in an Intrinsically Disordered Transcription Factor. Elife 2017, 6, 1–17.

(49). Baruffini E; Ferrari J; Dallabona C; Donnini C; Lodi T Polymorphisms in DNA Polymerase γ Affect the MtDNA Stability and the NRTI-Induced Mitochondrial Toxicity in Saccharomyces Cerevisiae. Mitochondrion 2015, 20, 52–63. [PubMed: 25462018]

Author Manuscript Author Manuscript Author Manuscript Author Manuscript

(50). Chan SSL; Copeland WC DNA Polymerase Gamma and Mitochondrial Disease: Understanding the Consequence of POLG Mutations. Biochim. Biophys. Acta – Bioenerg 2009, 1787 (5), 312–319.

Author Manuscript Author Manuscript Author Manuscript Author Manuscript

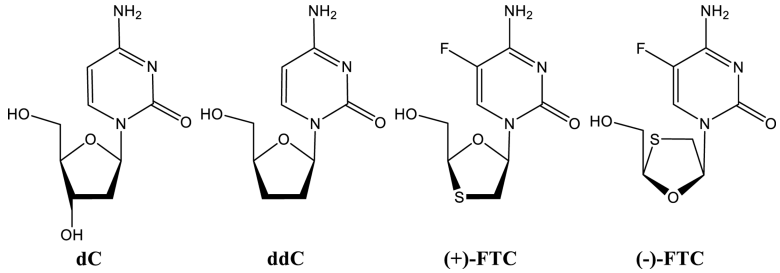

Figure 1.

Structures of natural substrate deoxycytidine and nucleoside reverse transcriptase inhibitors (NRTI).

Author Manuscript Author Manuscript Author Manuscript Author Manuscript

A

Range	A	B	C	D	E	F
Residue	271 - 311	403 - 468	793 - 822	844 - 925	973 - 1054	1082 - 1122
Domain	Exo	Exo	Pol	Pol	Pol	Pol
Annotation	Motif IV	Motif III & Thumb (440-475)	Thumb (785-815)	Palm/ Fingers (910-1095	Fingers	Palm/ Fingers

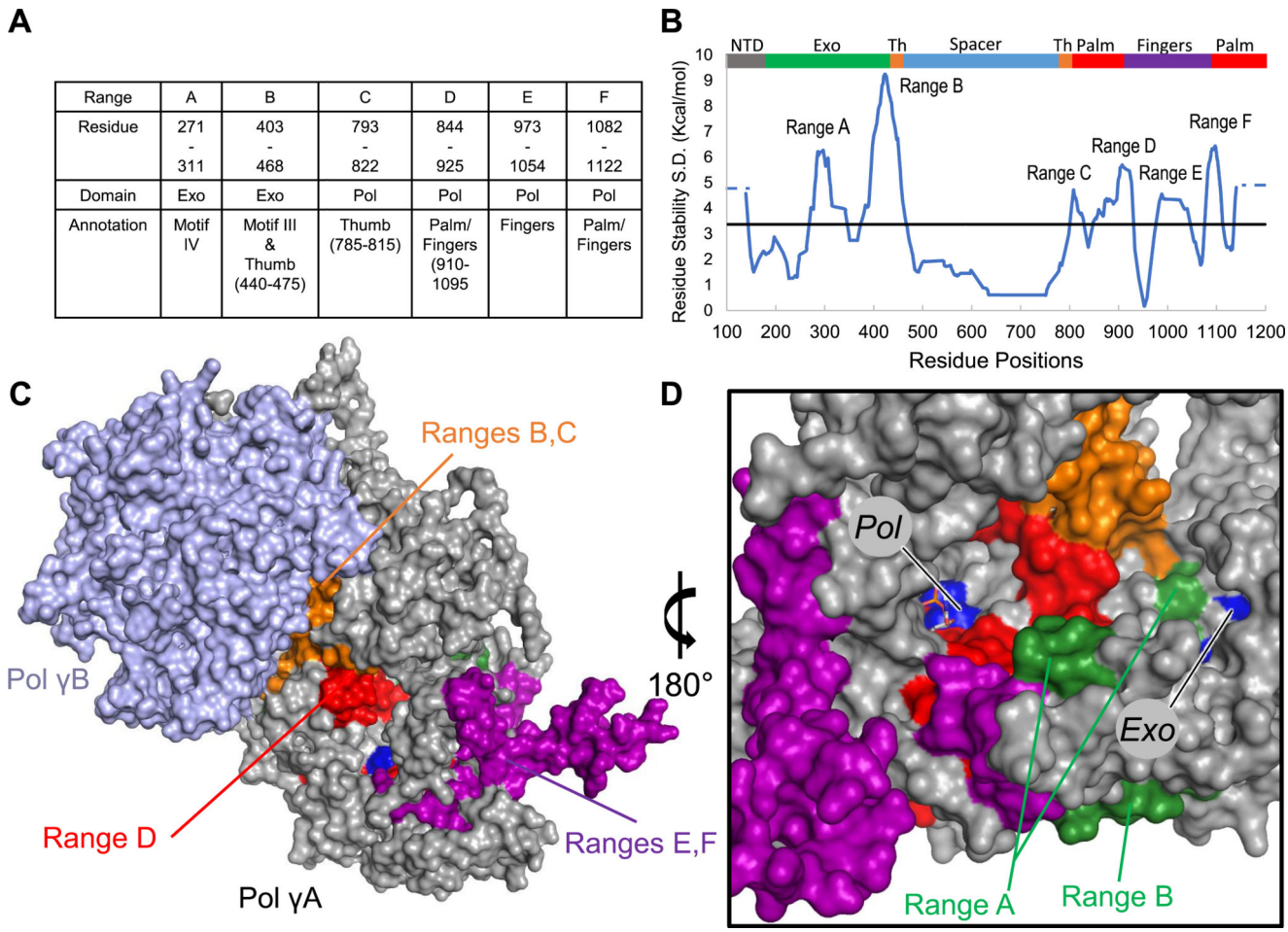

Figure 2.

Different dNTP/NRTI perturb local and nonlocal regions of Pol γ. (A) The hypervariable regions are shown in the table along with their domain, subdomain, and motif associations.[20,21] (B) Population standard deviation (S.D.) of residue stability for each complex is plotted as the regional average of 30 amino acids, and the horizontal line is the average SD. The N and C termini were not considered hypervariable and so are shown instead as dotted lines. Gray is the N-terminal domain (1–170), green the 3′−5′ exonuclease (170–440), orange the thumb subdomain (440–475 and 785–815), blue the spacer (475–815), red the palm (815–910 and 1095–1239), and purple is the fingers subdomain (910–1095) of *pol*. (C,D) Ranges A–F are mapped onto the ternary structure (PDB: 4ZTZ) and colored based upon domain assignment (DNA not shown), Pol γA is shown in gray, and Pol γB subunits are shown in light blue. The perturbed thumb domain interacts with Pol γB subunit, which may affect enzyme processivity. (D) Most perturbed residues lie between the two active sites. Active site residues are colored in blue and labeled according to their respective active site, while the dCTP substrate is shown as sticks.

Author Manuscript Author Manuscript Author Manuscript Author Manuscript

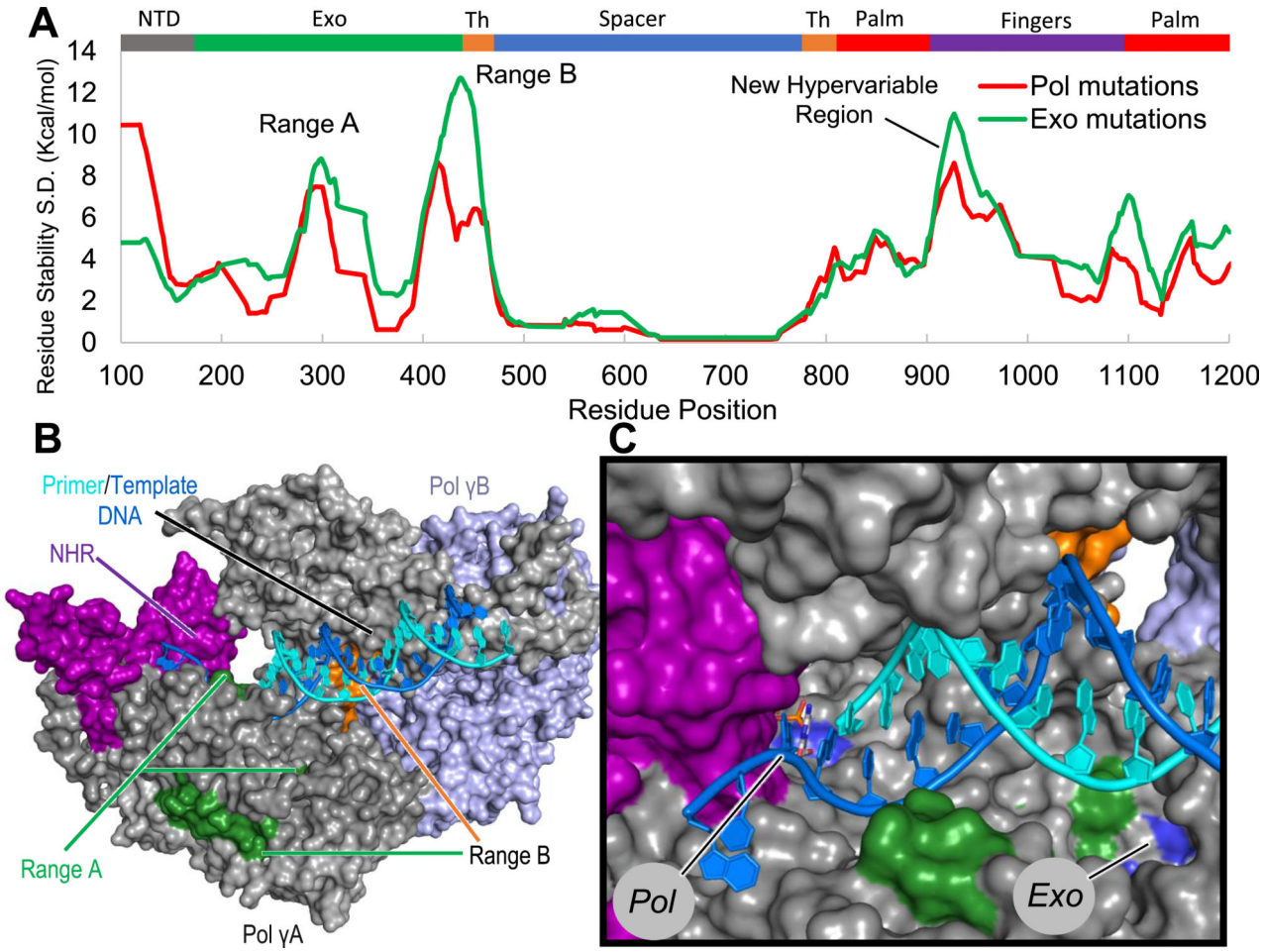

Figure 3.

In silico *pol* and *exo* mutations suggest cooperativity between active sites. We find that either *exo* or *pol* mutations perturb local and nonlocal regions. This includes residues adjacent to active site residues. (A) Residue stability SD is plotted with finger and *exo* domain mutations in red and green, respectively. A regional average of 30 amino acids was used. (B,C) Hypervariable regions displayed are ranges A, B, and residues 900–1050 referred to as the new hypervariable region (NHR). These are mapped on the Pol γ complex according to the domain/subdomain coloring scheme.

Author Manuscript Author Manuscript Author Manuscript Author Manuscript

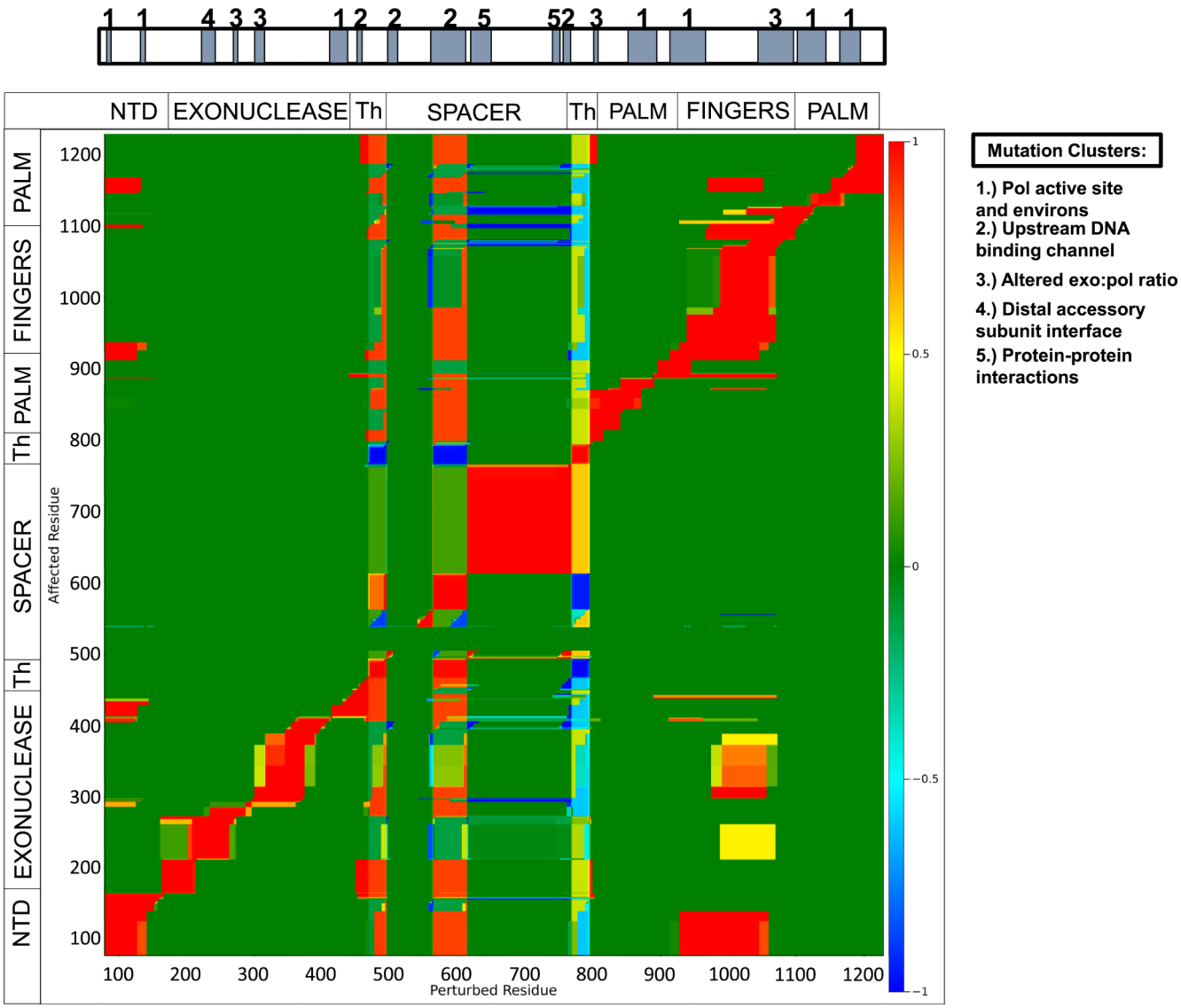

Figure 4.

Allosteric network connectivity map reveals a cooperative network. The X-axis represents perturbed residues and the Y-axis denotes the corresponding affected residues. A color scale is shown on the right where red is highly positively cooperative, blue is negatively cooperative, and green represents no cooperativity; units are kcal/mol. Shown above are mutational clusters identified by Nurminen et al.[7]

Author Manuscript Author Manuscript Author Manuscript Author Manuscript

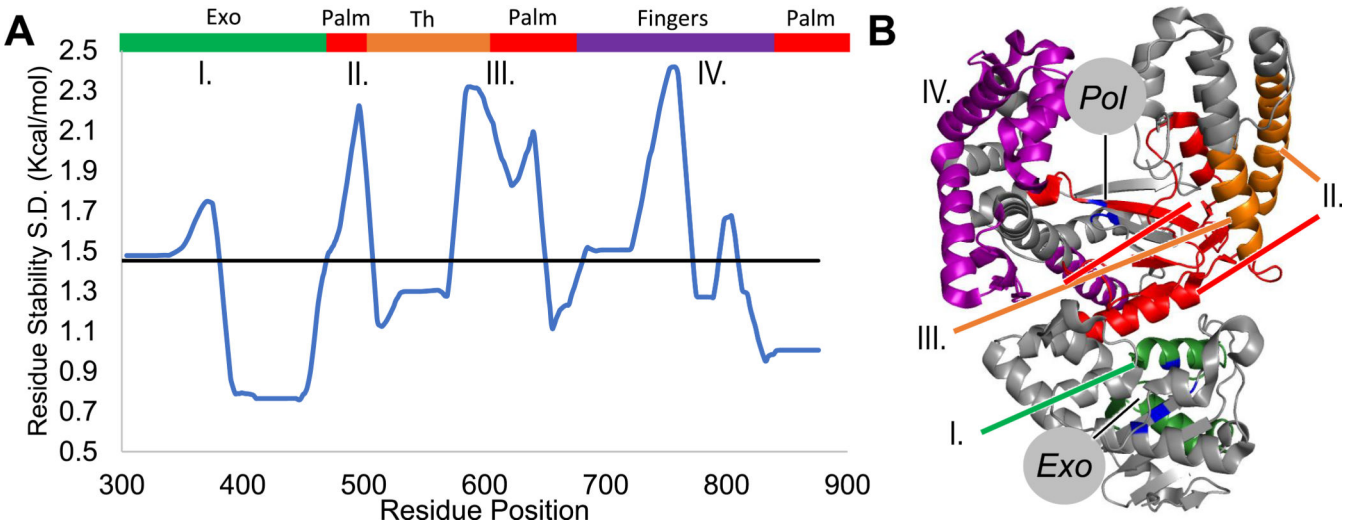

Figure 5.

Pol I BF mismatches show similarly perturbed domains as Pol γ. (A) Residue stability is plotted as a regional average of 15 residues, and the following domains and subdomains are displayed above: 3′−5′exonuclease domain (302–468), fingers (656–815), thumb (496–595), and palm (617–655 and 830–869). Mean residue stability is shown as a horizontal line in black. (B) Regions shown to be hypervariable are mapped on the crystal structure with the DNA not shown (PDB: 1L3U). Hypervariable regions (residue stability greater than the mean) are colored based upon domain association. Catalytic residues are in blue.